KAMPALA INTERNATIONAL UNIVERSITY

KIU
Journal of Science, Engineering and Technology

KJSET

Research Article

Development of an optimized virtual inertia control strategy for frequency stability in a Two-Area Microgrid System

Mugisha Simon[1], Abdullahi Bala Kunya[2], Bubu Pius Erheyovwe[3]

Department of Electrical, Telecommunication and Computer Engineering, Kampala International University, Uganda[1]

Department of Electrical Engineering, Kabale University, Kabale-Uganda[2]

simon.mugisha@studwc.kiu.ac.ug [1,2], abkunya@kiu.ac.ug [2], bubupius.e@.kiu.ac.ug [3]

Corresponding Author: simon.mugisha@studwc.kiu.ac.ug [1]

Paper history:
Received 22 April 2026
Accepted in revised form 04 June 2026

Keywords
Virtual Inertia Control, Frequency regulation, Two-area microgrid, Control area, Fuzzy-PID, ISE optimization, tie-line

Abstract

The increasing penetration of inverter-based renewable energy sources has significantly reduced inertia in modern microgrids, resulting to large frequency deviations. The conventional load frequency control methods are insufficient in such low inertia microgrids as they depend on the inherent inertia of the synchronous generators. This thesis presents the development of an optimized virtual inertia control strategy for frequency stability in a low inertia two-area microgrid system. A two-area microgrid system incorporating the diesel engine generators, wind turbines, photovoltaic systems and battery energy storage systems was modelled using the state-space mathematical model approach. The virtual inertia was emulated through the power electronic interfaces and controller parameters through fuzzy logic. The fuzzy-PID controller was evaluated under two distinct load disturbance scenarios using MATLAB/Simulink (R2024b). The simulation results demonstrate the optimized controller significantly reduces the frequency deviations, undershoot and overshoot amplitudes, and achieves faster settling time compared to conventional PID controller.

Nomenclature and units

VIC	Virtual Inertia Control
PID	Proportional Integral Derivative
ISE	Integral Square Error
ACE	Area Control Error
Hz	Hertz

1.0 Introduction

In Power System, grid support services are essential for maintaining power system stability and power quality. Among these services, frequency regulation is key to ensuring continuous equilibrium between power supply and load to sustain the nominal system frequency (Annamraju & Nandiraju, 2018; Saxena *et al*., 2022). In interconnected systems, frequency regulation minimizes frequency deviations and controls tie-line power exchanges between control areas through coordinated operation of generators and spinning reserves (Aemro *et al*., 2020; Mo *et al*., 2019a).

Inverter-Based Energy Sources such as photovoltaic systems, wind turbine and fuel cells interface with the grid through power electronic converters that lack mechanical inertia. Consequently, these systems exhibit low inertia and weak frequency response, making them more susceptible to rapid frequency deviations and instability (Nour *et al*., 2023).

The rapid incorporation of inverter-based energy sources (IES) like photovoltaic systems and wind turbines has significantly reduced the overall inertia of modern power systems (Al Kez *et al*., 2023). Unlike conventional synchronous generators, IES interface with the grid through power electronic converters, which do not inherently provide physical inertia (Song *et al*., 2023). As a result, the system becomes increasingly vulnerable to frequency instability following disturbances or load changes. This challenge is particularly severe in islanded microgrids, where the absence of strong interconnections and reliance on inverter-dominated exacerbate the effects of low inertia. Even minor disturbances in such systems can lead to large and rapid frequency deviations, potentially resulting in equipment damage, load shedding, or total system collapse (Hasheminasab *et al*., 2024).

To overcome these limitations, the virtual inertia has been introduced. This enables inverter-based resources to mimic behaviour of synchronous machines by momentarily altering their output power in response to frequency deviations. This synthetic inertial support enhances frequency stability and resilience in low-inertia microgrids, bridging the gap between conventional high-inertia systems and emerging inverter-dominated power networks (Khazali *et al*., 2022a; Mo *et al*., 2019b; Munoz *et al*., 2022a).

2.0 System modelling

This section presents the dynamic models of diesel engine generator, wind turbine, photovoltaic and battery energy storage system.

2.1 State-space modelling

The system is designed with two control areas interconnected with a tie-line as shown in Figure 1.

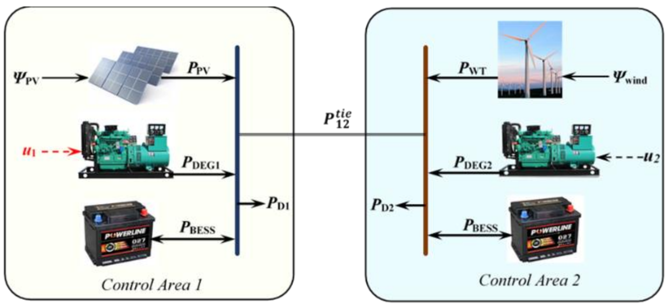

Figure 1: The proposed microgrid system

A set of first order differential equations defined (1)-(13) is used to describe the dynamics of the system shown in Figure 2.

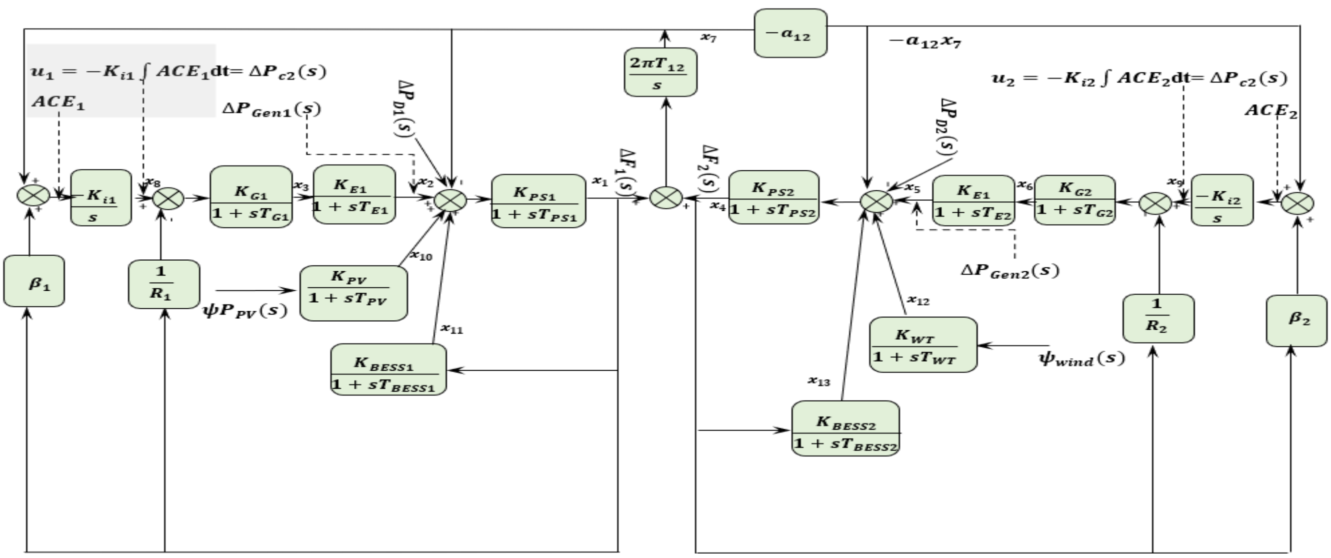

Figure 2: State-Space Model of Two-Area System

$x_1 = \Delta f_1$ is the frequency change in area 1,

$x_2 = \Delta P_{Gen1}$ is the change in power generation in area 1,

$x_4 = \Delta f_2$ is the frequency change in area 2,

$x_5 = \Delta P_{Gen2}$ is the change of power generation in area 2,

$x_8 = \int ACE_1$ is the ACE of area 1,

$x_9 = \int ACE_2$ is the ACE of area 2,

$u_1 = \Delta P_{C1}$ is the control signal for area 1,

$u_2 = \Delta P_{C2}$ is the control signal for area 2,

$w_1 = \Delta P_{D2}$ is the load change in area 1,

$w_2 = \Delta P_{D2}$ is the load change in area 2

$$\dot{x}_1 = -\frac{1}{T_{PS1}}x_1 + \frac{K_{PS1}}{T_{PS1}}x_2 - \frac{K_{PS1}}{T_{PS1}}x_7 + \frac{K_{PS1}}{T_{PS1}}x_{10} + \frac{K_{PS1}}{T_{PS1}}x_{11} - \frac{K_{PS1}}{T_{PS1}}w_1 \tag{1}$$

$$\dot{x}_2 = -\frac{1}{T_{E1}}x_2 + \frac{1}{T_{E1}}x_3 \tag{2}$$

$$\dot{x}_3 = -\frac{1}{R_1 T_{G1}}x_3 - \frac{1}{T_{G1}}x_3 + \frac{1}{T_{G1}}u_1 \tag{3}$$

$$\dot{x}_4 = -\frac{1}{T_{PS2}}x_4 + \frac{K_{PS2}}{T_{PS2}}x_5 + a_{12}\frac{K_{PS2}}{T_{PS2}}x_7 + \frac{K_{PS2}}{T_{PS2}}x_{12} + \frac{K_{PS2}}{T_{PS2}}x_{13} - \frac{K_{PS2}}{T_{PS2}}w_2 \tag{4}$$

$$\dot{x}_5 = -\frac{1}{T_{E2}}x_5 + \frac{1}{T_{E2}}x_6 \tag{5}$$

$$\dot{x}_6 = -\frac{1}{R_2 T_{G2}}x_4 - \frac{1}{T_{G2}}x_6 + \frac{1}{T_{G2}}u_2 \tag{6}$$

$$\dot{x}_7 = 2\pi T_{12}x_1 - 2\pi T_{12}x_4 \tag{7}$$

$$\dot{x}_8 = \beta_1 x_1 + x_7 \tag{8}$$

$$\dot{x}_9 = \beta_2 x_4 - a_{12}x_7 \tag{9}$$

$$\dot{x}_{10} = -\frac{1}{T_{PV}}x_{10} + \frac{1}{T_{PV}}\psi P_{PV} \tag{10}$$

$$\dot{x}_{11} = -\frac{1}{T_{BESS1}}x_{11} + \frac{1}{T_{BESS1}}x_1 \tag{11}$$

$$\dot{x}_{12} = -\frac{1}{T_{WT}}x_{12} + \frac{1}{T_{WT}}\psi_{wind} \tag{12}$$

$$\dot{x}_{13} = -\frac{1}{T_{BESS2}}x_{13} + \frac{1}{T_{BESS2}}x_2 \tag{13}$$

Rearranging equations (1)-(13) in matrix form, the state-space model of a two-area microgrid system is formulated as shown in equations (14) and (15).

$$\dot{X} = Ax(t) + Bu(t) + P_1\Delta P(t) + Fw(t) \tag{14}$$

$$
\begin{pmatrix}\dot{x}_1\\ \dot{x}_2\\ \dot{x}_3\\ \dot{x}_4\\ \dot{x}_5\\ \dot{x}_6\\ \dot{x}_7\\ \dot{x}_8\\ \dot{x}_9\\ \dot{x}_{10}\\ \dot{x}_{11}\\ \dot{x}_{12}\\ \dot{x}_{13}\end{pmatrix}
=
\begin{pmatrix}
-\frac{1}{T_{PS1}} & \frac{K_{PS1}}{T_{PS1}} & 0 & 0 & 0 & 0 & -\frac{K_{PS1}}{T_{PS1}} & 0 & 0 & \frac{K_{PS1}}{T_{PS1}} & \frac{K_{PS1}}{T_{PS1}} & 0 & 0\\
0 & -\frac{1}{T_{E1}} & \frac{1}{T_{E1}} & 0 & 0 & 0 & 0 & 0 & 0 & 0 & 0 & 0 & 0\\
-\frac{1}{R_1 T_{G1}} & 0 & -\frac{1}{T_{G1}} & 0 & 0 & 0 & 0 & 0 & 0 & 0 & 0 & 0 & 0\\
0 & 0 & 0 & -\frac{1}{T_{PS2}} & \frac{K_{PS2}}{T_{PS2}} & 0 & \frac{a_{12}K_{PS2}}{T_{PS2}} & 0 & 0 & 0 & 0 & 0 & 0\\
0 & 0 & -\frac{1}{T_{E2}} & \frac{1}{T_{E2}} & 0 & 0 & 0 & 0 & 0 & 0 & 0 & 0 & 0\\
0 & 0 & -\frac{1}{R_2 T_{G2}} & 0 & -\frac{1}{T_{G2}} & 0 & 0 & 0 & 0 & 0 & 0 & 0 & 0\\
2\pi T_{12} & 0 & 0 & -2\pi T_{12} & 0 & 0 & 0 & 0 & 0 & 0 & 0 & 0 & 0\\
\beta_1 & 0 & 0 & 0 & 0 & 0 & 1 & 0 & 0 & 0 & 0 & 0 & 0\\
0 & 0 & 0 & \beta_2 & 0 & 0 & -a_{12} & 0 & 0 & 0 & 0 & 0 & 0\\
0 & 0 & 0 & 0 & 0 & 0 & 0 & 0 & 0 & -\frac{1}{T_{PV}} & 0 & 0 & 0\\
\frac{1}{T_{BESS1}} & 0 & 0 & 0 & 0 & 0 & 0 & 0 & 0 & 0 & -\frac{1}{T_{BESS1}} & 0 & 0\\
0 & 0 & 0 & 0 & 0 & 0 & 0 & 0 & 0 & 0 & 0 & -\frac{1}{T_{WT}} & 0\\
0 & \frac{1}{T_{BESS2}} & 0 & 0 & 0 & 0 & 0 & 0 & 0 & 0 & 0 & 0 & -\frac{1}{T_{BESS2}}
\end{pmatrix}
\begin{pmatrix}x_1\\ x_2\\ x_3\\ x_4\\ x_5\\ x_6\\ x_7\\ x_8\\ x_9\\ x_{10}\\ x_{11}\\ x_{12}\\ x_{13}\end{pmatrix}
$$

$$
+\begin{pmatrix}
0 & 0\\ 0 & 0\\ \frac{1}{T_{G1}} & 0\\ 0 & \frac{1}{T_{G2}}\\ 0 & 0\\ 0 & 0\\ 0 & 0\\ 0 & 0\\ 0 & 0\\ 0 & 0\\ 0 & 0\\ 0 & 0\\ 0 & 0
\end{pmatrix}
\begin{pmatrix}u_1\\ u_2\end{pmatrix}
+\begin{pmatrix}
0 & 0 & 0 & 0\\ 0 & 0 & 0 & 0\\ 0 & 0 & 0 & 0\\ 0 & 0 & 0 & 0\\ 0 & 0 & 0 & 0\\ 0 & 0 & 0 & 0\\ 0 & 0 & 0 & 0\\ 0 & 0 & 0 & 0\\ 0 & 0 & 0 & 0\\ \frac{1}{T_{PV}} & 0 & 0 & 0\\ 0 & 0 & 0 & 0\\ 0 & 0 & \frac{1}{T_{WT}} & 0\\ 0 & 0 & 0 & 0
\end{pmatrix}
\begin{pmatrix}\psi P_{PV}\\ \Delta P_{\mathrm{BESS1}}\\ \psi_{\mathrm{wind}}\\ \Delta P_{BESS2}\end{pmatrix}
+\begin{pmatrix}
-\frac{K_{PS1}}{T_{PS1}} & 0\\ 0 & 0\\ 0 & 0\\ 0 & -\frac{K_{PS2}}{T_{PS2}}\\ 0 & 0\\ 0 & 0\\ 0 & 0\\ 0 & 0\\ 0 & 0\\ 0 & 0\\ 0 & 0\\ 0 & 0\\ 0 & 0
\end{pmatrix}
\begin{pmatrix}w_1\\ w_2\end{pmatrix}
\quad (15)
$$

3.0 Controller design

This section presents the structure of the controller and the fuzzy logic controller base rules.

3.1 The controller structure

The load frequency controller was designed on PID-based framework and the controller modulates the synthetic inertia provided by BESS in response to the frequency deviations. The fuzzy logic controller receives the Area Control Error (ACE) as its input and generates a tuning signal that adjusts the PID controller as shown in Figure 3. Seven triangular membership function were used to represent the linguistic variables Negative Big (NB), Negative Medium (NM), Negative Small (NS), Zero (Z), Positive Small (PS), Positive Medium (PM), and Positive Big (PB) over a normalized range of -1 to 1. The membership functions were designed with greater density near zero to improve sensitivity around the nominal operating point, which enhances frequency stabilization in the microgrid system.

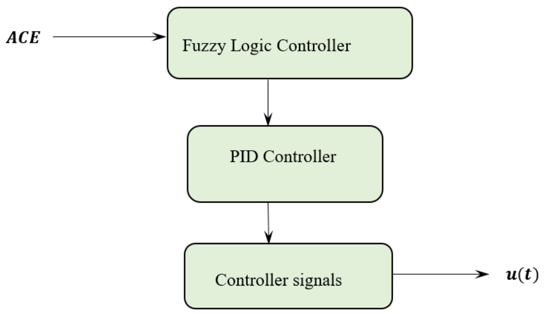

Figure 3: The controller design

3.2 The fuzzy logic controller rules

The fuzzy rule base in Table 1 defines the relationship between the ACE, change in ACE and the PID tuning signal. The rule base consists of 49 IF-THEN rules derived from expert knowledge of load frequency controller behaviour. Each rule determines the appropriate tuning action of the PID controller based on the magnitude and direction of the system error. Large deviations in ACE result in strong control actions, while small deviations produce mild adjustments to avoid oscillations. This rule base enables the fuzzy controller to enhance the dynamic response and stability of the two-area microgrid system.

Table 1: The fuzzy logic controller base rules

ACE/ΔACE	**NB**	**NM**	**NS**	**Z**	**PS**	**PM**	**PB**
NB	NB	NB	NM	NM	NS	Z	Z
NM	NB	NM	NM	NS	Z	PS	PS
NS	NM	NM	NS	Z	PS	PM	PM
Z	NM	NS	Z	Z	Z	PS	PM
PS	NS	Z	PS	PS	PM	PM	PB
PM	Z	PS	PM	PM	PM	PB	PB
PB	Z	PS	PM	PM	PB	PB	PB

4.0 Results and discussion

This section presents the effectiveness of the load frequency control strategy was evaluated using time-domain simulations in MATLAB/Simulink (R2024b) on a two-area microgrid system. This was carried out under two distinct scenarios which include; scenario I which involves single step load perturbation to assess system resilience during a sudden 0.1 pu load increase in single control area, and scenario II, double step load perturbation to test the robustness of the controller against successive disturbances occurring in both control areas at different intervals.

4.1 Two-area microgrid system

The two control areas are connected together through the tie-line for power exchange, and control objective is to regulate the frequency deviations and tie-line power oscillations in both areas under load/renewable disturbances. The two area are combined as subsystems i.e. Area 1 and Area 2 as shown in Figure 4.

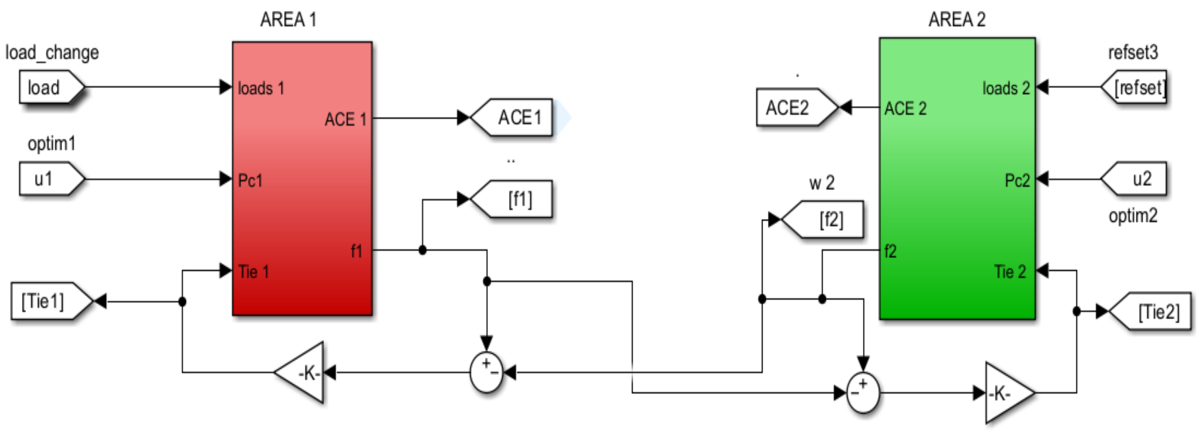

Figure 4: The 2-CA microgrid simulink model

4.2 Fuzzy-PID controller design

The ACE1 membership function in Figure 5 represents the fuzzy interpretation of the ACE in CA1. The horizontal axis shows the normalized ACE1 range from -1 to 1, the vertical axis represents the degree of membership between 0 and 1. Seven triangular membership functions were used to describe the linguistic variables NB, NM, NS, Z, PS, PM, and PB, corresponding to different magnitudes of the control error. When ACE1 is strongly negative (NB or NM), it indicates a large power deficit in area1, meaning generation must increase to restore frequency stability. As the error approaches zero (Z), the system moves towards its steady-state operating condition, and minimal control action is required. Positive ACE1 values (PS, PM, PB) indicate excess generation in area1, requiring a reduction in generation output. The triangular shapes overlap smoothly to ensure gradual transitions between control actions, enabling the fuzzy controller to respond effectively to disturbances while maintaining stable operation of the microgrid system.

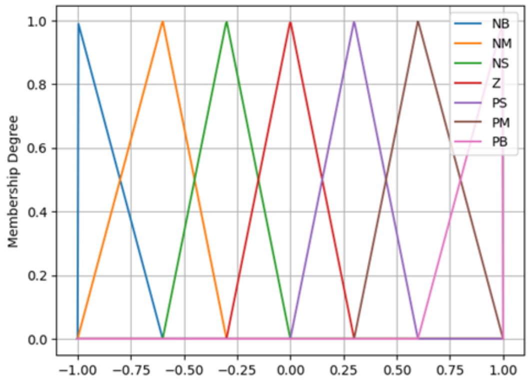

Figure 5: Fuzzy membership functions

The ACE_2 membership function in Figure 6 represents the fuzzy characterization of the ACE in CA2. Similar to ACE 1, the input variable is defined over the normalized interval from -1 and 1 and uses seven triangular membership functions representing NB, NM, NS, Z, PS, PM, and PB. These linguistic variables allow the fuzzy controller to evaluate the severity and direction of the system imbalance in area 2. When ACE 2 takes large negative values, the membership functions NB or NM become dominant, indicating insufficient power generation in area 2 and triggering corrective control actions through the PID controller. Conversely, large positive ACE 2 values correspond to excess generation, requiring the controller to reduce power output. Near the center region (Z), the system operates close to equilibrium, and only minimal control effort is applied. The symmetric and overlapping triangular membership functions ensure smooth transitions between adjacent states, improving the dynamic response and stability of the systemThe fuzzy inference system employs seven triangular membership functions (NB, NM, NS, Z, PS, PM, PB) defined over the normalized range -1 to 1 as shown in Figure 7. These membership functions convert the PID tuning signal into linguistic variables, enabling smooth rule-based adjustment of controller parameters and improving frequency regulation performance of the two-area microgrid system.

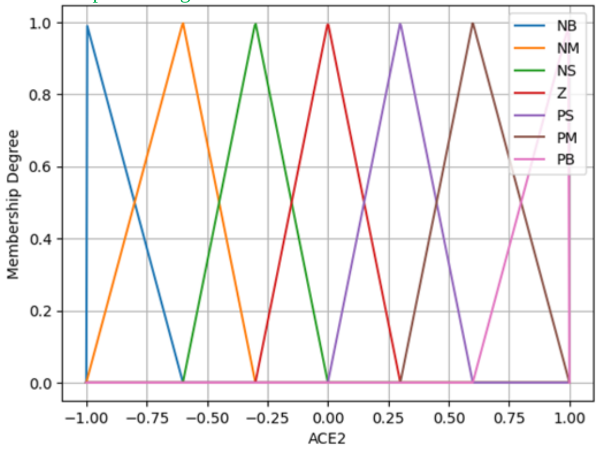

Figure 6: Fuzzy membership function for ACE2

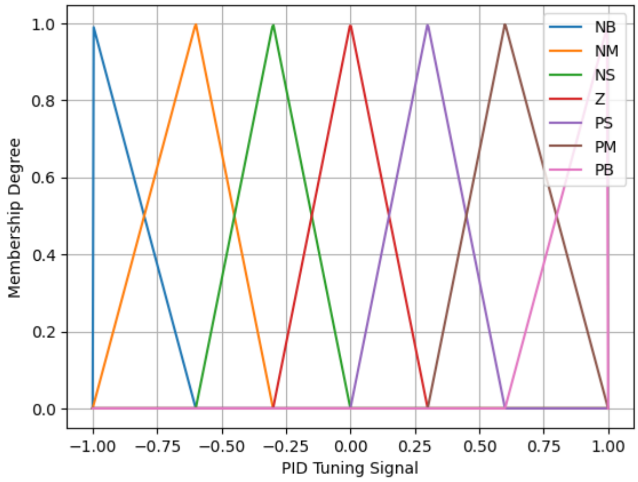

Figure 7: Fuzzy membership functions for PID control output

The frequency control strategy in Figure 8 combines a fuzzy logic system to dynamically tune the gains of a conventional PID controller, making the PID more robust and adaptive, essentially marrying the simplicity of PID with the intelligence of fuzzy logic for superior, self-tuning performance in complex scenarios.

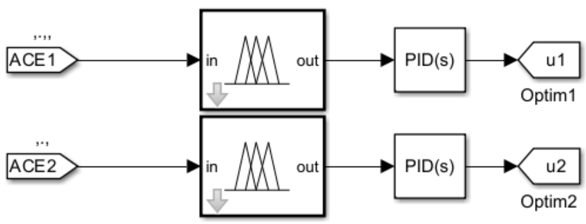

Figure 8: The Fuzzy-PID Controller

4.3 Performance evaluation under different operating conditions

This section presents the two distinct scenarios used to evaluate the effectiveness of the controller. These scenarios include; a single-step load perturbation and double-step load perturbation. The time-domain simulations were performed on the two-area microgrid system using MATLAB/Simulink (R2024b). In both cases, the system responses were compared with those obtained using a conventional PID controller, with settling time, tie-line power, frequency and undershoot serving as the key performance metrics.

i. Single-Step Load Perturbation (SSLP)

In the first scenario, only Control Area 1 (CA1) is subjected to a 0.1 pu step load increase applied at 5 s, while Control Area 2 (CA2) remains undisturbed, as shown in Figure 9. The dynamic responses of the system are analyzed for both the proposed fuzzy-based PID controller and the conventional PID controller.

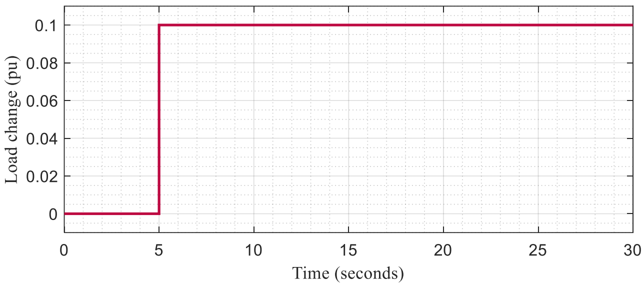

Figure 9: Single-Step Load Perturbation

When the application of step load is carried out, the transient response reveals clear performance differences between the two controllers. The conventional PID exhibits a deeper frequency nadir of -0.291 Hz compared to the fuzzy PID's smaller dip of -0.168 Hz. Following the nadir, the conventional PID produces a higher positive overshoot in the range of +0.12 Hz and settles at 6.81 sec, whereas the fuzzy PID limits it to +0.04 Hz with settling time of 5.28 sec. In terms of oscillatory behaviour, the conventional PID response is characterized by larger oscillations and slower damping as shown in Figure 10, while the fuzzy PID significantly reduces the oscillation amplitude and damps them out more quickly. Although both controllers eventually eliminate steady-state error due to the integral action, the fuzzy PID achieves faster settling as shown in Table 2 with less overshoot and undershoot indicating superior transient performance as shown in Table 3.

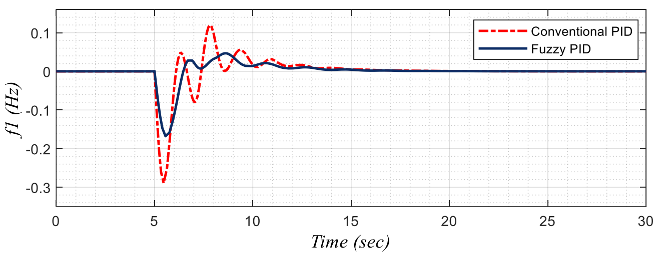

Figure 10: CA1 Frequency response after Single area disturbance

Even though the CA2 is left undisturbed, the single area load disturbance causes the power imbalance across the entire interconnection, affecting the frequency in CA2. This makes the conventional PID controller to experience an undershoot of -0.120 Hz while fuzzy PID controller experiences an undershoot of -0.068 Hz. The Conventional PID exhibits a significant overshoot. After the frequency reaches its lowest point (-0.1 Hz), the controller action is too aggressive, causing the frequency to swing above the nominal setpoint (0 Hz) to a peak of approximately +0.05 Hz. This overshoot is undesirable as it stresses the generating units. The fuzzy PID controller shows dramatically reduced overshoot as the frequency response approaches the setpoint smoothly without crossing it significantly. This shows a much more damped and controlled response. The conventional PID exhibits the response oscillating around the setpoint for a period of 6.47 sec whereas the fuzzy PID shows the response converging towards the zero deviation with settling time of 4.88 sec, achieving the steady state faster than the conventional PID as shown in Figure 11.

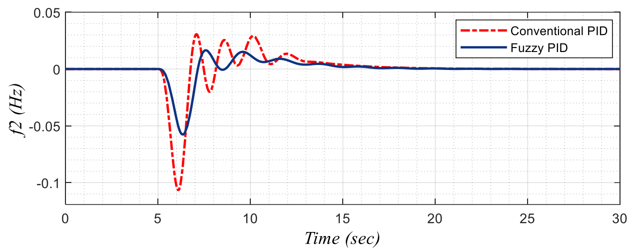

Figure 11: CA2 Frequency response without Single area disturbance

The response of the tie-line power flow in Figure 12 shows a clear superiority of the fuzzy PID controller over the conventional PID in managing the interconnection following a disturbance. The conventional PID response is characterized by significant undershoot and pronounced overshoot, leading to sustained oscillations that take a long time to dissipate, resulting in a lengthy settling time of 5.98 sec as shown in Table 2. In contrast, the fuzzy PID controller effectively minimizes both undershoot and overshoot with settling time of 4.56 sec as shown in Figure 12, producing a smooth, well-damped response that returns the tie-line power to its scheduled value with fewer oscillations. This allows the fuzzy PID to achieve a much faster settling time shown in Table 2, indicating a more stable and efficient restoration of power balance between the two control areas (CA1 and CA2).

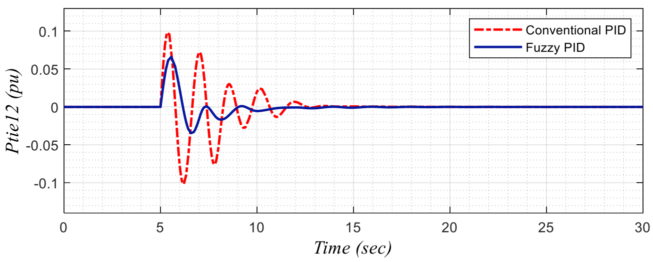

Figure 12: Tie-line power response after Single area disturbance

ii. Double-Step Load Perturbation (DSLP)

In the second scenario, CA1 is initially disturbed with a 0.1 pu step load at 0 sec as shown in Figure 13. Subsequently, at 15 s, CA2 is also subjected to a 0.2 pu step load. This case is designed to assess the ability of the proposed control scheme to effectively handle both single and successive disturbances.

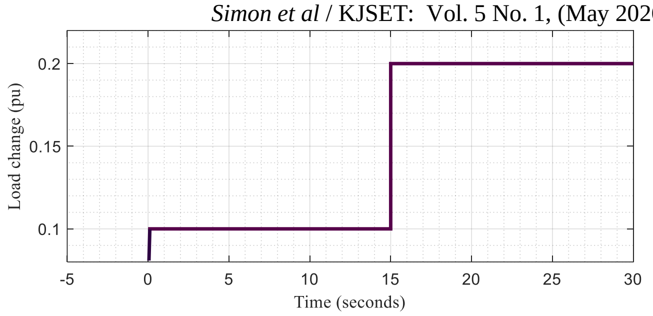

Figure 13: Double Area Load Change (Disturbance)

When CA2 experiences a 0.1 pu disturbance at 0 sec, tie-line oscillates strongly. Conventional PID shows higher peaks with an overshoot of +0.009 pu and an undershoot of -0.01 pu, before gradually stabilizing. At 15 sec, the 0.2 pu disturbance in CA2 again triggers large oscillations with similar amplitude and the settling occurs at about 6 sec. In contrast, fuzzy PID limits the deviations with a smaller overshoot of +0.005 pu and undershoot of -0.005 pu. It damps oscillations more quickly after both disturbances and this gives a settling time of about 4.5 sec. Therefore, the fuzzy PID improves damping and inter-area power stability by minimizing oscillation magnitude and stabilizing the frequency of the system faster shown in Figure 14.

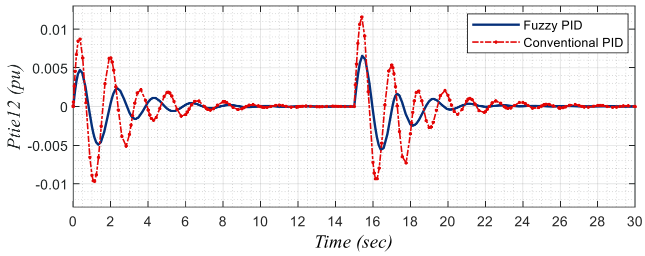

Figure 14: Tie-line power response after Double area disturbance

For the frequency deviation in CA1 shown in Figure 14, conventional PID controller yields an initial undershoot of -0.0105 Hz and an overshoot of +0.006 Hz, and following the second disturbance at 15 sec, the undershoot reaches 0.010 Hz with settling time of about 6.8 sec. In contrast, the fuzzy PID significantly improves the response with the initial undershoot reduced to 0.0065 Hz and overshoot to +0.0048 Hz while the second disturbance is also managed more smoothly with a settling of about 5.3 sec. Therefore, the fuzzy PID enhances frequency stability in CA1 by reducing both overshoot/undershoot and settling time.

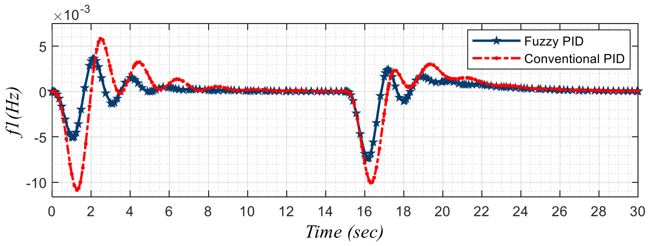

Figure 14: CA1 Frequency response after Double area disturbance

For the frequency deviation in CA2 shown in Figure 15, conventional PID produces larger oscillations with an initial undershoot of -0.038 Hz and a maximum overshoot of about +0.018 Hz and when the second disturbance is applied, oscillations intensify before damping out within 6.5 sec while fuzzy PID reduces the undershoot to -0.028 Hz and overshoot to about +0.013 Hz, with quicker damping with settling time of about 4.9 sec and therefore fuzzy PID controller provides a much smoother frequency regulation in CA2 ensuring faster system frequency stability.

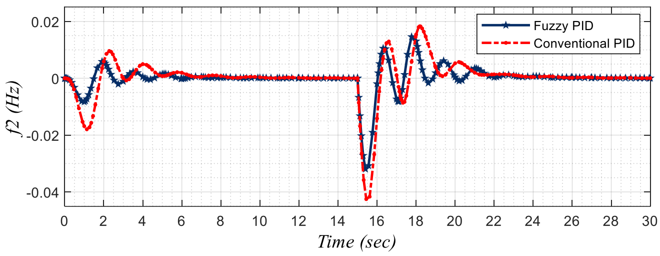

Figure 15: CA2 Frequency response after Double area disturbance

4.4 Comparative analysis of fuzzy-PID controller against conventional PID controller

The Table 2 summarizes the settling time performance of the two controllers for frequency deviations in CA1, CA2 and the tie-line power flow. It is clear that the proposed fuzzy-based PID controller consistently outperforms the conventional PID in all cases. In CA1, the settling time reduces from 6.81 sec with the conventional PID to 5.28 sec with the fuzzy-PID, yielding an improvement to 22.52%. Similarly, in CA2, the fuzzy PID controller achieves a faster stabilization at 4.88 sec compared to 6.47 sec, corresponding to an improvement of 24.64%. In the case of tie-line power flow, the settling time is decreased from 5.98 sec to 4.56 sec, yielding an enhancement of 23.85%. These confirm that the fuzzy-PID enhances system dynamics by providing faster stabilization, improved damping and more efficient disturbance rejection than the conventional PID controller.

Table 2: Summary of the comparative analysis on the setting time

Responses	Settling time (*sec*)		Improvement
	Conv-PID	Fuzzy-PID	
f_1	6.81	**5.28**	22.52%
f_2	6.47	**4.88**	24.64%
P_{tie12}	5.98	**4.56**	23.85%

For frequency deviation in CA1, the undershoot improves from 0.291 Hz with conventional PID to -0.168 Hz with fuzzy PID, representing a 42.27% enhancement. Similarly, CA2, undershoot decreases from -0.120 Hz to -0.068 Hz, which shows an improvement of 43.33% as shown Table 3. This shows that the fuzzy PID controller provides faster recovery and less severe dip in frequency following a disturbance.

However, the tie-line power deviation shows a different trend where the undershoot increases from 0.072 pu with conventional PID to 0.095 pu with fuzzy PID, resulting in a 31.94% deterioration rather than improvement as shown in Table 3. Therefore, this shows while the fuzzy PID controller is more effective in stabilizing the frequency responses of the two control areas, it slightly compromises tie-line power deviation performance. The comparative analysis of undershoot values that the fuzzy-PID controller significantly reduces undershoot in the system response compared to the conventional PID controller. To balance the performance on the tie-line, further tunning may be required.

Table 3: Summary of the comparative analysis on the undershoot

Responses	**Undershoot**		**Improvement**
	Conv-PID	**Fuzzy-PID**	
f_1 ***(Hz)***	-0.291	**-0.168**	42.27%
f_2 ***(Hz)***	-0.120	**-0.068**	43.33%
P_{tie12} ***(pu)***	0.072	**0.095**	31.94%

5.0 Discussion of findings

To further validate the effectiveness of the proposed optimized fuzzy-PID controller, its performance is quantitatively compared with results reported in previous LFC studies involving conventional PID, fuzzy-based controllers, and optimization-based intelligent controllers in two-area interconnected systems.

Most classical two-area LFC studies such as those based on the standard model presented by (Kothari & Nagrath, 2003) report settling times typically between 6-12 seconds under 0.1 pu step disturbances when using conventional PID controllers. More recent intelligent controller studies report improvements ranging from 15-35% depending on the optimization strategy used. Therefore, this study shows improvements exceeding 22-24% in settling time and over 40% reduction in frequency undershoot, which are consistent with many reported results in literature.

i. **The structural validation of the developed model**

The developed model has 13 state variables ($\boldsymbol{x_1}$ through $\boldsymbol{x_{13}}$). If BESS, PV and WT are excluded from the system, the matrix, A reduces exactly to standard 7-state two area microgrid system. Therefore, the developed model is the extended form of the standard system and the structural formulation is correct.

The tie-line equation of the developed model matches with the classical tie-line equation in (Kothari & Nagrath, 2003) and therefore the tie-line modelling is correct.

ii. ***Comparison of settling time***

Table 4 compares the settling time improvement achieved in this study with results commonly reported in similar two-area LFC systems.

Table 4: Comparison of settling time with literature

Method	**Disturbance(pu)**	**Settling time(s)**	**Improvement over PID (%)**
Conventional PID (Classical LFC models)	0.1	6-10	-------
Fuzzy controller (reported in LFC studies)	0.1	5-8	15-25
PSO-PID (optimization-based LFC)	0.1	4.8-6	18-30
Proposed Fuzzy-PID-PSO (CA1)	0.1	**5.28**	**22.52**
Proposed Fuzzy-PID-PSO (CA2)	0.1	**4.88**	**24.64**
Tie-line power (This study)	0.1	**4.56**	**23.85**

The results demonstrate that the proposed controller performs within the upper performance range reported in literature. The settling time reductions achieved in CA1 and CA2 exceed 22%, confirming strong damping enhancement. Compared to classical PID-based LFC systems, the proposed method provides significantly faster stabilization.

iii. ***Comparison of frequency undershoot(nadir)***

Table 5: Comparison of frequency undershoot with literature

Method	**Frequency undershoot (Hz)**	**Reduction (%)**
Conventional PID (Typical two-area LFC)	-0.25 to -0.35	----------
Fuzzy-based LFC (reported studies)	-0.18 to -0.22	20-35
PSO-optimized PID	-0.16 to -0.20	30-40
Proposed fuzzy-PID-PSO (CA1)	**-0.168**	**42.27**

Proposed fuzzy-PID-PSO (CA2)	**-0.068**	**43.33**

The proposed controller achieves over 40% reduction in frequency undershoot, which exceeds the typical improvements reported for standalone fuzzy or PSO-based controllers. This confirms that combining adaptive fuzzy tuning with PSO optimization enhances disturbance rejection capability in low-inertia microgrids.

iv. Comparison of tie-line power oscillation

Table 6: Comparison of tie-line power performance

Method	Settling time (s)	Oscillation magnitude	Observation
Conventional PID	6-9	High	Poor damping
Fuzzy LFC	5-7	Moderate	Improved damping
Optimization-based LFC	4.5-6	Low	Good damping
Proposed method	**4.56**	**Low (but slight undershoot increase)**	**Faster stabilization**

Although the proposed controller significantly improves settling time and damping of tie-line oscillations, a slight increase in undershoot magnitude was observed compared to the conventional PID. Similar trade-offs have been reported in literature where optimization objectives prioritize frequency deviation over-line oscillation minimization.

6.0 Conclusion

This study successfully developed, designed and validated an optimized virtual inertia control strategy for frequency stability in a low inertia two-area microgrid system. The controller was validated under single-step and double-step load disturbances and compared against a conventional PID controller using key performance indices such as settling time, undershoot, oscillatory behavior and overshoot.

7.0 Future work

To extend the scope of this research, future work could focus on several key areas. First, experimental validation of the controller using hardware-in-the-loop or real-time simulation platforms would provide practical insights beyond simulation-based results. Additionally, extending the proposed control strategy to larger multi-area or interconnected microgrid systems would help assess its scalability and effectiveness in more complex configurations. Further investigations should also consider the impact of communication delays, measurement noise, and cyber-physical constraints on load frequency control, as these factors are critical in real-world deployments. Finally, incorporating renewable energy uncertainties such as variable wind speed and solar irradiance would allow for a more comprehensive evaluation of the controller's robustness under realistic operating conditions.

8.0 References

Annamraju, A., & Nandiraju, S. (2018). Frequency control in an autonomous two-area hybrid microgrid using grasshopper optimization based robust PID controller. *2018 8th IEEE India International Conference on Power Electronics (IICPE)*, 1–6.

Aemro, Y. B., Moura, P., & de Almeida, A. T. (2020). Design and modeling of a standalone Dc-Microgrid for off-grid schools in rural areas of developing countries. *Energies*, *13*(23), 6379.

Nour, M., Magdy, G., Bakeer, A., Telba, A. A., Beroual, A., Khaled, U., & Ali, H. (2023). A new fractional-order virtual inertia support based on battery energy storage for enhancing microgrid frequency stability. *Fractal and Fractional*, *7*(12), 855.

Al Kez, D., Foley, A. M., Ahmed, F., & Morrow, D. J. (2023). Overview of frequency control techniques in power systems with high inverter-based resources: Challenges and mitigation measures. *IET Smart Grid*, *6*(5), 447–469.

Song, J., Zhou, X., Zhou, Z., Wang, Yang, Wang, Yifan, & Wang, X. (2023). Review of Low Inertia in Power Systems Caused by High Proportion of Renewable Energy Grid Integration. *Energies*, *16*(16). https://doi.org/10.3390/en16166042

Hasheminasab, S., Alzayed, M., & Chaoui, H. (2024). A review of control techniques for inverter-based distributed energy resources applications. *Energies*, *17*(12), 2940.

Khazali, A., Rezaei, N., Saboori, H., & Guerrero, J. M. (2022a). Using PV systems and parking lots to provide virtual inertia and frequency regulation provision in low inertia grids. *Electric Power Systems Research*, *207*, 107859.

Mo, W., Walker, P. D., & Zhang, N. (2019). Dynamic analysis and control for an electric vehicle with harpoon-shift synchronizer. *Mechanism and Machine Theory, 133*, 750-766.

Muñoz, P. E., González, S. A., & Mantz, R. J. (2022). Distributed generation contribution to primary frequency control through virtual inertia and damping by reference conditioning. *Electric Power Systems Research*, *211*, 108168.

Chen, T., Guo, J., Chaudhuri, B., & Hui, S. (2020). Virtual inertia from smart loads. *IEEE Transactions on Smart Grid*, *11*(5), 4311–4320.

Guo, W., & Mu, L. (2016). Control principles of micro-source inverters used in microgrid. *Protection and Control of Modern Power Systems*, *1*(1), 5.

Chen, X., Jiang, Y., Terzija, V., & Lu, C. (2024). Review on measurement-based frequency dynamics monitoring and analyzing in renewable energy dominated power systems. *International Journal of Electrical Power & Energy Systems*, *155*, 109520.

Zhang, Z., & Babayomi, O. (2024). Distributed Secondary Control of Microgrids with Inertia Emulation. In

Community Energy and Microgrids: Control, Operation and Optimization (pp. 49–68). Springer.

Zhang, X., Li, D., Yang, Z., Tian, L., Meng, J., Liu, Y., & Fu, C. (2023). Fuzzy adaptive virtual inertia control of energy storage systems considering SOC constraints. *Energy Reports*, *9*, 2431–2439.

Zhang, Y., Liu, X., & Qu, B. (2017). Distributed model predictive load frequency control of multi-area power system with DFIGs. *IEEE/CAA Journal of Automatica Sinica*, *4*(1), 125–135.

Idan, R., Mahdi, A., Wahhab, T. A., & others. (2023). Review on virtual inertia control topologies for improving frequency stability of microgrid. *Eng. Technol. J*, *41*(2), 345–358.

Jiang, C., Cai, G., Yang, D., Liu, X., Hao, S., & Li, B. (2024). Multi-objective configuration and evaluation of dynamic virtual inertia from DFIG based wind farm for frequency regulation. *International Journal of Electrical Power & Energy Systems*, *158*, 109956.

Heidary, J., Gheisarnejad, M., Rastegar, H., & Khooban, M. H. (2022). Survey on microgrids frequency regulation: Modeling and control systems. *Electric Power Systems Research*, *213*, 108719.

Djaraf, N., Daili, Y., Zemmit, A., & Harrag, A. (2025). Fuzzy-Virtual inertia control to improve the frequency response of multi-area power systems. *Turkish Journal of Electrical Engineering and Computer Sciences*, *33*(2), 145–166.

Hosseini, S. A. (2024). Frequency control using electric vehicles with adaptive latency compensation and variable speed wind turbines using modified virtual inertia controller. *International Journal of Electrical Power & Energy Systems*, *155*, 109535.

Jafari, M., Gharehpetian, G. B., & Anvari-Moghaddam, A. (2024). On the role of virtual inertia units in modern power systems: A review of control strategies, applications and recent developments. *International Journal of Electrical Power & Energy Systems*, *159*, 110067.

Jianfang, X., Peng, W., Setyawan, L., Chi, J., & Hoong, C. F. (2015). Energy management system for control of hybrid AC/DC microgrids. *2015 IEEE 10th Conference on Industrial Electronics and Applications (ICIEA)*, 778–783.

Li, Q., Ren, B., Tang, W., Wang, D., Wang, C., & Lv, Z. (2022). Analyzing the inertia of power grid systems comprising diverse conventional and renewable energy sources. *Energy Reports*, *8*, 15095–15105.

Mitali, J., Dhinakaran, S., & Mohamad, A. (2022). Energy storage systems: A review. *Energy Storage and Saving*, *1*(3), 166–216.